Supramolecular Nanostructures of 1,3,5-Benzene-tricarboxylic Acid at Electrified Au(111)/0.05 M H_2SO_4 Interfaces: An in Situ Scanning Tunneling Microscopy Study

Z. Li, B. Han, L. J. Wan,† and Th. Wandlowski*

Institute of Thin Films and Interfaces, ISG 3, and Center of Nanoelectronic Systems for Information Technology, Research Center Jülich, D-52425 Jülich, Germany

Received March 23, 2005. In Final Form: May 11, 2005

The potential-induced adsorption and self-assembly of 1,3,5-benzene-tricarboxylic acid (TMA) was investigated at the electrified Au(111)/0.05 M H_2SO_4 interface by in-situ scanning tunneling microscopy (STM) and surface enhanced infrared reflection absorption spectroscopy (SEIRAS) in combination with electrochemical techniques. Depending on the applied electric field, TMA forms five distinctly different, highly ordered supramolecular adlayers on Au(111) surfaces. We have elucidated their real-space structures at the molecular scale. In the potential range $-0.25\ \text{V} < E < 0.20\ \text{V}$, planar-oriented TMA molecules form a hexagonal open-ring honeycomb structure, Ia, $\begin{pmatrix} 6 & 6 \\ 0 & 6 \end{pmatrix}$, a hydrogen-bonded ribbon-type phase, Ib, $\begin{pmatrix} 10 & -4 \\ 7 & 7 \end{pmatrix}$, and a herringbone-type phase, Ic, $\begin{pmatrix} 14 & 0 \\ 7 & 13 \end{pmatrix}$, stabilized by directional hydrogen bonding and weak substrate−adsorbate interactions. Interfacial water molecules are being replaced. In $0.20\ \text{V} \leq E < 0.40\ \text{V}$, e.g., around the potential of zero charge, and at slightly higher coverages, a close-packed physisorbed adlayer of hydrogen-bonded TMA dimers, II, $\begin{pmatrix} 0 & 5 \\ 4 & 4 \end{pmatrix}$, was observed. Further increase of the electrode potential to positive charge densities causes an orientation change from planar to upright. An initially disordered phase, IIIa, transforms into an ordered, stripelike chemisorbed adlayer, IIIb, $\begin{pmatrix} 3 & 0 \\ 4 & 8 \end{pmatrix}$, of perpendicularly oriented TMA molecules. One carboxylate group per molecule is bound to the electrode surface, while the two other protonated carboxyl groups are directed toward the electrolyte and act as structure-determining components of a hydrogen-bonded two-dimensional ladder-type network. Structural transitions between the various types of ordered molecular adlayers are attributed to (hole) nucleation and growth processes.

1. Introduction

The self-assembly of organic supramolecular nanostructures is based on noncovalent interactions such as hydrogen-bonding, π-stacking, and van der Waals forces or metal ion ligand coordination as found in proteins, nucleic acids, liquid crystals, and molecular complexes.[1] The spontaneous generation of organized structures depends on the design of molecular components capable of self-assembling into supramolecular entities. The nature of the species obtained is determined by the information stored in the individual components. Self-assembly methods represent a unique potential to create well-defined functional structures with dimensions on the nanometer scale and to control surface properties. The assembly of supramolecular structures via hydrogen-bonding has developed into a central theme for constructing a wide variety of molecular nanostructures in solution, in liquid crystals, in the solid state, and on surfaces.[2] Hydrogen bonds are formed when a donor (D) with an available acidic hydrogen atom is brought into direct contact with an acceptor (A). Hydrogen bonding is not random but selective and controlled by the directional strength of intermolecular interactions.[3] It can be used to tune the spatial arrangement of functionalized molecules and ions in the solid state and on surfaces. The structural and energetic features of hydrogen-bonding interactions have been extensively studied.[4−9] The choice of molecular shape and size and especially the arrangement of hydrogen-bonding donor and acceptor sites are crucial to the correct tessellation of tailored supramolecular arrays.

Carboxylic acids are commonly used as motif-controlling functional elements in crystal engineering. They can form hydrogen-bonding patterns that contain a center of symmetry, the *dimer motif*, and also aggregate in acentric one-dimensional chains, *catemers*, resulting from the formation of hydrogen bonds to two or more neighboring acids.[9] The dimer synthon has been used to assemble a variety of supermolecules due to its bidentate character, which increases the strengths of interactions considerably. For example, terephthalic acid (1,4-benzene-dicarboxylic

* Author to whom correspondence should be addressed. E-mail: th.wandlowski@fz-juelich.de. Web: http://www.fz-juelich.de/isg/index.php?index=239.

† Center of Molecular Sciences, Institute of Chemistry, Chinese Academy of Sciences, Beijing 100080, People's Republic of China.

(1) Lehn, J. M. *Supramolecular Chemistry*; Wiley-VCH: Weinheim, 1995.

(2) *Comprehensive Supramolecular Chemistry*; Atwood, L. J., Davies, J. E. D., MacNicols, D. D., Vögtle, F., Lehn, J. M., Eds., Pergamon: New York, 1996.

(3) Etter, M. C. *Acc. Chem. Res*. **1990**, *23*, 120.

(4) Desiraju, G. R. *Crystal Engineering*; Elsevier: Amsterdam, 1989.

(5) *Chem. Mater.* **1994**, *6* (8).

(6) Jeffrey, G. A.; Saenger, W. *Hydrogen Bonding in Biological Structures*; Springer: Berlin, 1991.

(7) Subramanian, S.; Zaworotko, M. J. *Coord. Chem. Rev*. **1994**, *137*, 357.

(8) MacDonald, J. G.; Whitesides, G. M. *Chem. Rev*. **1994**, *94*, 2383.

(9) Melendez, R.; Hamilton, A. D. *Top. Curr. Chem*. **1998**, *198*, 97.

10.1021/la0507737 CCC: $30.25
Published on Web 06/11/2005

acid, TA)[10] and isophthalic acid (1,4-benzene-dicarboxylic acid, IA)[11] form one-dimensional tapes and ribbons, respectively. Trimesic acid (1,3,5-benzene-tricarboxylic acid, TMA) with its 3-fold molecular symmetry forms a two-dimensional network composed of characteristic honeycomb units.[12−14] The ∼1.4 nm diameter cavities of the honeycombs are often employed to fabricate inclusion compounds.[15,16] TMA represents a prototype material for supramolecular self-assembly. The acid and some analogue structural motifs have been used as template patterns to create a variety of nanostructures.[9,15−22] Functionalized TMA,[23] its protonated forms,[24] and its metal complexes[21,25,26] were employed as unique building blocks in crystal engineering. The ordering at surfaces was recently studied under UHV conditions[27,28] and at the solid−liquid interface.[29,30] Molecular self-assembly at surfaces is governed by the subtle balance between intermolecular and molecule−surface interactions, which can be tuned by the substrate material and symmetry, the temperature or, at electrified interfaces, by the applied electrode potential. Dmitriev et al.[27] reported on Cu(100) at low temperatures (∼200 K) the existence of 2D ordered adlayer islands composed of a honeycomb structure of TMA molecules in a planar orientation. Long-range order was not achieved due to kinetic limitations. At room temperature, deprotonation of the carboxyl groups leads to an upright adsorption geometry, where chemisorbed TMA molecules are anchored to the substrate through a carboxylate functionality. The upright molecules order in striped islands. Barth et al. also explored the molecular assembly of metal−organic coordination networks of TMA and related aromatic carboxylic acids on well-defined metal surfaces in ultrahigh vacuum.[31] Griessl et al.[28] reported on HOPG at 25 K up to room temperature the coexistence of two hexagonal ring structures composed of TMA with hydrogen bonds formed either between two (honeycomb pattern) or three (flower structure) adjacent molecules.

Alternatively, the adsorption-triggered self-assembly of TMA[29,30,32] and many other monomeric precursors[33,34] can be explored on well-defined conducting surfaces in an electrochemical environment. This approach offers the advantage, in comparison to a UHV-based environment, that formation, properties, and structural transitions of a wide variety of 2D supramolecular adlayers can be tuned (and equilibrated!) by the applied electrode potential and subsequently characterized by structure-sensitive in-situ techniques in real space and real time.[33,34] Ishikawa et al. reported for Au(111)/0.1 M $HClO_4$ a honeycomb-type (8×8) 2D network of flat oriented TMA molecules, which transform at higher potentials into a close-packed structure of TMA dimers.[29] Under rather similar experimental conditions, Su et al. found three ordered TMA adlayers.[30] A quasi-hexagonal (4×4) phase of planar oriented molecules at low coverages and negative charge densities changes via a mixed ($5 \times 2\sqrt{3}$) adlayer into a high-coverage striped phase at rather high positive potentials. The latter is ascribed to perpendicularly adsorbed TMA molecules coordinated with one or two deprotonated carboxylate groups to the positively charged electrode. The authors discuss two separate domains, which were approximated by ($2\sqrt{3} \times 4\sqrt{3}$) or ($7 \times 2\sqrt{3}$), respectively, giving rise to a surface concentration of 2.9 10^{-10} mol cm^{-2}. The different results of the two groups might be related to kinetically controlled structure transformations of the respective adlayers and/or of the substrate surface, especially when considering the rather low TMA concentration of 0.1 mM employed in both reports. This constellation motivated us to carry out a comprehensive electrochemical in-situ STM and spectroscopic study on steady-state patterns and the dynamics of potential-induced supramolecular ordering of TMA adlayers on Au(111)−(1×1) and Au(111)−($p \times \sqrt{3}$) surfaces.

The present paper is organized as follows. Experimental details are summarized in Section 2. Then we report on the steady-state properties of potential-dependent interfacial structures of trimesic acid on Au(111) (Sections 3.1 and 3.2). Kinetic aspects of adlayer phase formation processes will be explored in Section 3.3. The in-situ STM results will be compared with IR spectroscopic investigations employing surface enhanced infrared spectroscopy (ATR−SEIRAS[32]).

2. Experimental Section

Electrolyte Solutions and Single-Crystal Experiments. The electrolyte solutions were prepared with Milli-Q water (18 MΩ, 2 ppb TOC), H_2SO_4, HCl (suprapure Merck), and trimesic acid (for synthesis, Lancaster, twice recrystallized). All electrolytes were deareated with argon before and during the experiment. The measurements were carried out at 20 ± 0.5 °C. The glassware was cleaned either in caroic acid or in a 1:1 mixture of hot H_2SO_4 (95−97% pro-analysis, Merck) and HNO_3 (65% purissimum, Riedel-de-Haen) followed by extended rinsing with Milli-Q water.

The ideal Au(111) or stepped Au($n\ n\ n - 2$) electrodes were single-crystal cylinders of 4 mm height and 4 mm diameter. They were flame-annealed with a butane torch at red heat and then cooled in high-purity argon before immersion into ultrapure water. Contact with the electrolyte was always established under potential control in hanging meniscus configuration. Island-free Au(111)−(1×1) surfaces were prepared by the immersing of a freshly flame-annealed electrode under potential control at 0.50

(10) Bailey, M.; Brown, C. J. *Acta Crystallogr.* **1967**, *22*, 387.
(11) Alcala, R.; Martinez-Carrera, S. *Acta Crystallogr.* **1972**, *B28*, 1671.
(12) Duchamp, D. J.; March, R. E. *Acta Crystallogr*. **1969**, *B25*, 5.
(13) Zaworotko, M. J. *Chem. Commun*. **2001**, *1*, 1.
(14) Herbstein, F. H. *Top. Curr. Chem.* **1987**, *140*, 107.
(15) Herbstein, F. H. In *Comprehensive Supramolecular Chemistry*; Atwood, J. L., MacNicol, D. D., Vögtle, F., Lehn, J. M., Eds.; Pergamon: New York, 1996; Vol. 6, p 61.
(16) Herbstein, F. H.; Kapon, M.; Maor, I.; Reisner, G. M. *Acta Crystallogr.* **1981**, *B37*, 136.
(17) De Feyter, S.; Gasquiere, A.; Klapper, M.; Müllen, K.; De Schryver, F. C. *Nano Lett.* **2003**, *3*, 1485.
(18) De Feyter, S.; De Schryver, F. C. *Chem. Soc. Rev.* **2003**, *32*, 139.
(19) Rabe, J. P.; Buchholtz, S. *Science* **1991**, *253*, 424.
(20) Eichhorst-Gerner, K.; Stabel, A.; Moessner, G.; Declerq, D.; Valiyaveettil, S.; Enkelmann, V.; Müllen, K.; Rabe, J. P. *Angew. Chem., Int. Ed. Engl.* **1996**, *35*, 1492.
(21) Lin, N.; Dmitriev, A.: Weckesser, J.; Barth, J. V.; Kern, K. *Angew. Chem., Int. Ed.* **2002**, *41*, 4779.
(22) Ermer, O.; Neudörfl, J. *Chem. Eur. J*. **2001**, *7*, 4961.
(23) Kolotuchin, S. V.; Fenlon, E. E.; Wilson, S. R.; Loweth, C. J.; Zimmerman, S. C. *Angew. Chem., Int. Ed. Engl.* **1996**, *34*, 2654.
(24) Melendez, R. E.; Sharma, C. V. K.; Zaworotko, M. J.; Bauer, C.; Rogers, R. D. *Angew. Chem., Int. Ed. Engl.* **1996**, *35*, 2213.
(25) Yaghi, O. M.; Li, G.; Li, H. *Nature* **1995**, *378*, 703.
(26) Gutschke, S. O. H.; Molinier, M.; Powell, A. K.; Winpenny, R. E. P.; Wood, P. T. *Chem. Commun*. **1996**, 823.
(27) Dmitriev, A.; Lin, N.; Weckesser, J.; Barth, J. V.; Kern, K. *J. Phys. Chem. B* **2002**, *106*, 6907.
(28) Griessl, S.; Lackinger, M.; Edelwirth, M.; Hietschold, M.; Heckl, W. *Single Mol.* **2002**, *3*, 25.
(29) Ishikawa, Y.; Ohira, A.; Sakata, M.; Hirayama, C.; Kunitake, M. *Chem. Commun*. **2002**, 2652.
(30) Su, G. J.; Zhang, H. M.; Wan, L. J.; Bai, C. L.; Wandlowski, Th. *J. Phys. Chem. B* **2004**, *108*, 1931.
(31) Spillmann, H.; Dmitriev, A.; Lin, N.; Messina, P.; Barth, J. V.; Kern, K. *J. Am. Chem. Soc*. **2003**, *125*, 10725.
(32) Han, B.; Li, Z.; Pronkin, S.; Wandlowski, Th. *Can. J. Chem.* **2004**, *82*, 1481.
(33) Dretschkow, Th.; Wandlowski, Th. *Topics Appl. Phys.* **2003**, *85*, 259.
(34) Wandlowski, Th. In *Encyclopedia of Electrochemistry*, Gileadi, E., Urbakh, M., Eds, Wiley: New York, **2003**, p 383.

V (vs SCE) into deaerated 0.1 M HCl. After a waiting time of 60 s, the electrode was removed and thoroughly rinsed with Milli-Q water.[35] The custom-made electrochemical setup employed in this study was described in ref 36. All potentials in this paper are quoted with respect to a saturated calomel electrode (SCE).

Scanning Tunneling Microscopy. The STM experiments were carried out with a Molecular Imaging Pico SPM employing disk-shape Au(111) massive single crystals (10 mm diameter, 2 mm height). The STM tips were electrochemically etched tungsten tips (0.25 mm diameter) coated with polyethylene. Platinum wires served as quasi-reference and counter electrodes. All STM experiments were carried out at room temperature in constant-current mode with tunneling currents ranging between 3 and 200 pA.

Spectroelectrochemical Setup. The SEIRAS experiments were carried out with a Bruker IF 66v/s Fourier transform spectrometer synchronized with a Heka potentiostat PG 310 employing a vertical spectro-electrochemical cell in Kretschmann ATR configuration.[32,37] The spectrometer was operated in the slow-scan mode and for kinetic potential step experiments in the rapid-scan regime. The working electrode was a quasi-single crystalline Au(111−25 nm) film electrode prepared by electron beam evaporation of a thin gold film onto the (111) plane of a silicon hemisphere, and subsequent electrochemical annealing. The complete description of the spectroelectrochemical ATR−SEIRAS experiment and of the sample preparation is given in ref 32.

3. Results and Discussion

3.1. Electrochemical Data. Figure 1A shows a typical current vs potential curve of Au(111)−(1 × 1) in 0.05 M H_2SO_4 in the absence (dashed line) and in the presence of 3 mM TMA recorded with a scan rate of 10 mV s^{-1}. Under these conditions, TMA is completely protonated ($pK_1 = 2.1$, $pK_2 = 4.1$, $pK_3 = 5.18$).[38] The experiment started at 0.90 V with an unreconstructed, island-free surface, which was prepared by flame-annealing and subsequent electrochemical annealing in 0.1 M HCl.[35] The solid trace represents the first negative-going voltammetric cycle in the double layer region. Four characteristic potential regions (labeled I, II, IIIa, and IIIb in a sequence from lower to higher potentials), which are separated by the current peaks P1 | P1′, P2 | P2′, and P3 | P3′, can be readily distinguished. The stability range of I is delimited at negative potentials by the onset of hydrogen evolution and at positive potentials by the current peaks P1 | P1′. After a narrow region II, which is strongly dependent on scan rate and surface preparation (between P1 | P1′ and P2 | P2′), a broad current minimum develops in region IIIa. At more positive potentials, past the broad peak P3, a low-capacitance region, IIIb (saturation capacitance ∼10 μF cm^{-2}), is found. Upon increasing the potential further, the stability range of IIIb is delimited by the competing adsorption of OH^- and the onset of gold oxidation.

When starting the experiment at −0.10 V, e.g., at negative charge densities with a freshly flame annealed, reconstructed Au(111)−($p \times \sqrt{3}$) surface, a different voltammetric profile is obtained (Figure 1B). The first cycle (solid line) illustrates that P1 and P2 degenerate into shoulders, a new peak P4 appears, and upon changing the direction of the potential scan toward negative values, P1′ and P2′ broaden and nearly merge indicating the reduction of the stability range of II. Multiple cycling of the potential (dotted line in Figure 1B) leads to distinct

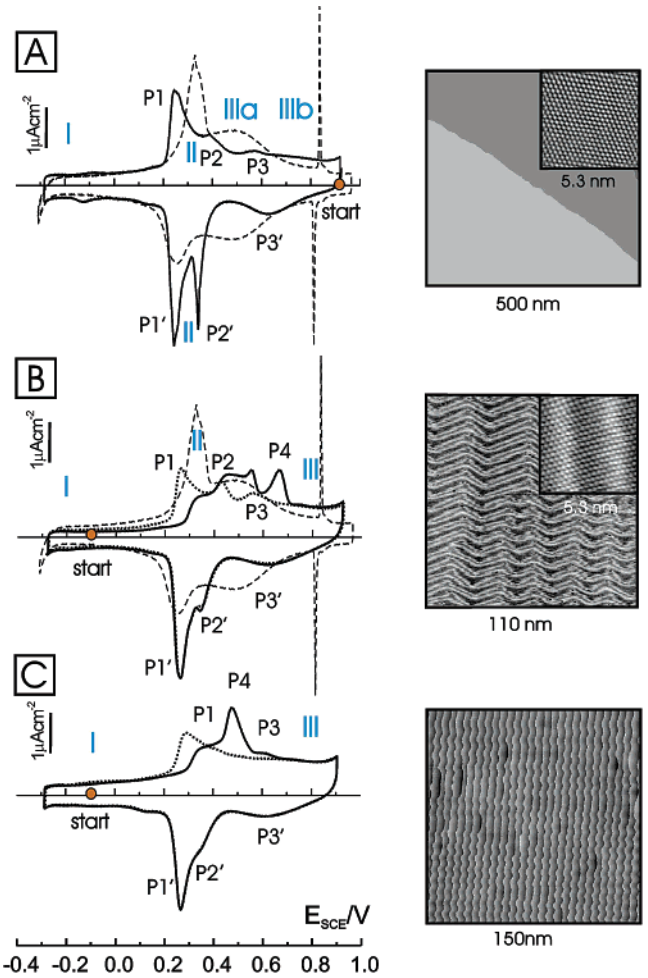

Figure 1. Cyclic voltammograms for gold electrodes in 0.05 M H_2SO_4 in the absence (dashed lines) and in the presence of 3 mM TMA (full lines, dotted lines), scan rate 10 mVs^{-1}. (A) Au(111)−(1 × 1); (B) Au(111)−($p \times \sqrt{3}$); (C) Au(111) −4° miscut along (110) with respect to the nominal (111) terrace orientation. The dotted traces represent the steady-state curves recorded after three complete potential cycles. The starting potentials of the various experiments are indicated by bold circles. The various adlayer regions are labeled I, II, IIIa, and IIIb. The right panels represent large-scale and atomic-resolution in-situ STM images of the various gold surfaces recorded at the individual starting potentials.

peaks P1, P2, and P3 in the positive-going scan direction; P4 disappears. No significant differences between the first and subsequent potential cycles were found in the traces representing the negative-going scan direction. We notice that the shapes of the current−potential curves recorded after multiple cycles with 10 mV s^{-1} in the double-layer region are not dependent on starting the experiment either with a freshly prepared Au(111)−(1 × 1) or with a reconstructed Au(111)−($p \times \sqrt{3}$) surface. This phenomenological description of the voltammetric profile plotted in Figure 1B indicates that P4 represents the charge due to lifting of the Au(111)−($p \times \sqrt{3}$) surface reconstruction.

Figure 1C shows the first voltammetric scan (solid line) and the quasi-steady-state curve (dotted line) measured after three subsequent potential cycles in −0.30 V < E < 0.90 V for a defect-rich Au(111) electrode (4° miscut with respect to the nominal (111) plane in the [110] direction). The previously introduced current peaks representing various structural transitions of the TMA adlayer respective the substrate surface decrease in magnitude and broaden (P1 | P1′, P2′, and P3 | P3′) or do not exist (P2). The lifting of the Au(111)−($p \times \sqrt{3}$) reconstruction (P4)

(35) Hölzle, M. H.; Wandlowski, Th.; Kolb, D. M. *J. Electroanal. Chem.* **1995**, *394*, 271.
(36) Pajkossy, T.; Wandlowski, Th.; Kolb, D. M. *J. Electroanal. Chem.* **1996**, *414*, 209.
(37) Wandlowski, Th.; Ataka, K.; Pronkin, S.; Diesing, D. *Electrochim. Acta* **2004**, *49*, 1233.
(38) *Lange's Handbook of Chemistry*, 13th ed.; Dean, J. A., Ed.; McGraw-Hill: New York, 1985; pp 5−42.

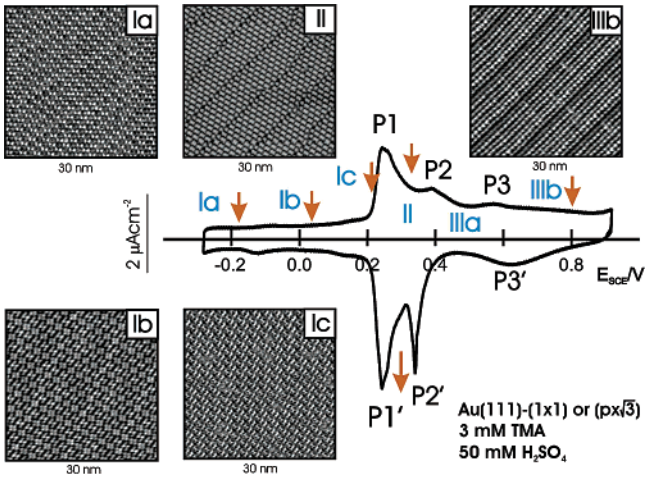

Figure 2. Steady-state voltammogram for Au(111) | 0.05 M H_2SO_4 in the presence of 3 mM TMA. The stability regions of the various adlayer phases are labeled Ia, Ib, Ic, II, IIIa, and IIIb, partially separated by the pairs of current peaks P1/P1′, P2/P2′, and P3/P3′, and they are illustrated with typical in-situ STM images: (Ia) hexagonal honeycomb phase, $E_s = -0.18$ V; (Ib) ribbon-type motif, $E_s = 0.03$ V; (Ic) herringbone motif, $E_s = 0.21$ V; (II) hydrogen-bonded linear dimers, $E_s = 0.34$ V; (IIIb) ordered chemisorbed striped phase of TMA at $E_s = 0.80$ V. Tunneling currents were below 200 pA.

occurs at lower potentials for the miscut surface, in comparison to the ideal terminated one, due to the negative shift of the potential of zero charge.[39]

The cyclic voltammograms of 3 mM TMA in 0.05 M H_2SO_4 (this work) and 0.1 M $HClO_4$[32] are rather similar except that the interfacial capacitances in regions IIIa and IIIb are slightly higher in sulfate-containing electrolyte, which is attributed to anion coadsorption in the Helmholtz region.[40]

3.2. In-Situ STM Studies—Steady State. *3.2.1. Overview.* Steady-state in-situ STM measurements were performed to explore structural details of the various stages of the electrochemical experiment. A carefully prepared unreconstructed Au(111)−(1 × 1) electrode was brought in contact with an electrolyte containing 0.05 M H_2SO_4 and 3 mM TMA under potential control at various potentials (Figure 1A). We observed no changes of the ideal terminated hexagonal substrate geometry, but five distinctly different supramolecular adlayer motifs depending on the applied potential and the assembly conditions (Figure 2). Three long-range, ordered adlayer structures were found in region I, the patterns of which we shall label honeycomb (structure Ia), ribbon-type (structure Ib), and herringbone-type (structure Ic). Region II is composed of strongly correlated chains of linear rows with characteristic translational domain boundaries (Figure 2, II). No ordered pattern was found at potentials between the current peaks P2 | P3 and P2′ | P3′. A striped phase with a rather regular variation in the STM contrast appears at $E >$ P3 (P3′) in potential region IIIb. Structural details of the five ordered TMA adlayers will be discussed next.

3.2.2. Hexagonal Honeycomb Phase Ia. Depositing TMA ($c > 0.2$ mM) from sulfuric acid solution on Au(111)−(1 × 1) at potentials more negative than 0.00 V, e.g., at a negatively charged electrode surface, gives rise to large domains (>100 nm) of a long-range, ordered honeycomb pattern. The latter represents a hexagonal network with equal-size cavities. No step decoration was found. The

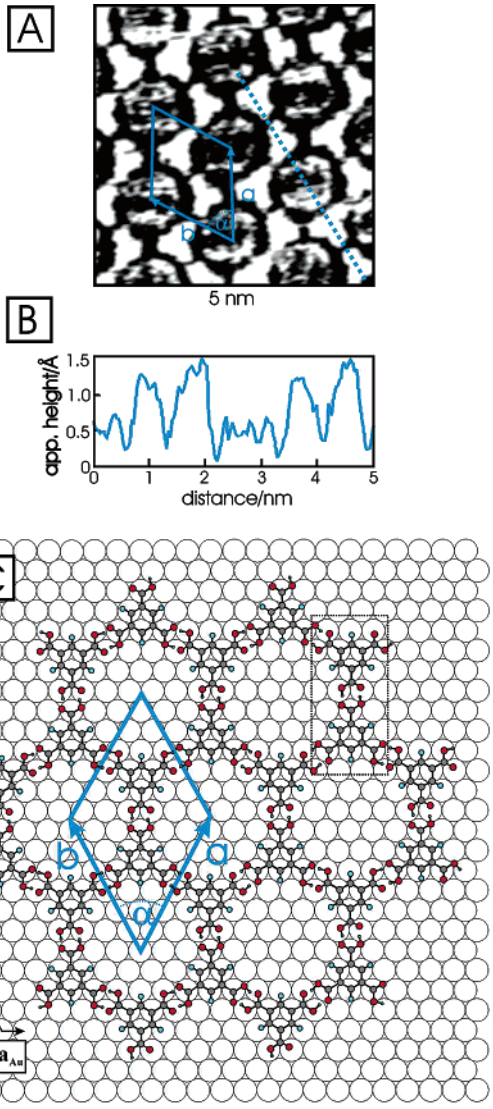

Figure 3. (A) High-resolution in-situ STM image of the hexagonal honeycomb phase Ia of TMA on Au(111) | 0.05 M H_2SO_4 in the presence of 3 mM TMA, $E_s = -0.10$ V, $i_T = 70$ pA. The primitive unit cell is indicated. (B) Typical cross-section profile along the cut indicated in (A). (C) Proposed packing model of TMA in Ia. The unit cell and a centrosymmetric dimer motif are indicated. The registry between the molecular adlayer and the substrate is based on the assumption that the phenyl rings of TMA are preferentially bound to high-symmetry 3-fold hollow sites of the Au(111) surface. The parameters of the unit cell are summarized in Table 1.

assembly process on terraces is rather slow. The rarely observed domain boundaries appear frizzy and do not strictly follow characteristic symmetry directions of the underlying Au(111) substrate surface, indicating a high mobility of TMA monomers and a rather weak adsorbate−substrate corrugation potential. Once formed, the TMA adlayer Ia is stable until the onset of hydrogen evolution at $E < -0.30$ V and at positive potentials up to the current peak P1 (Figure 2). We note that the same honeycomb structure of TMA is also observed on the reconstructed Au(111)−($p \times \sqrt{3}$) gold surface, without a preferential alignment to the substrate surface crystallography. High-resolution in-situ STM images (Figure 3A) reveal that the honeycomb pattern is composed of six bright, separately resolved triangular features, which are assigned to individual TMA molecules, and a dark depression in the center of the assembly. Their triangular contrast pattern with a characteristic side length of $l \approx 0.7-0.8$ nm and

(39) Lecoeur, J.; Rousset, S. *J. Electroanal. Chem.* **2002**, *519*, 18.
(40) Han, B.; Wandlowski, Th., unpublished, 2005.

Table 1. Characteristic Dimensions of the Unit Cell Parameters of the Various Ordered Adlayers Investigated for Au(111) | 0.05 M H_2SO_4 in the Presence of 3 mM TMA[a]

adlayer	*a* [nm]	*b* [nm]	*a* [deg]	area *A* per molecule [nm^2]	coverage Γ mol cm^{-2} 10^{10}
honeycomb Ia	1.70 ± 0.08	1.70 ± 0.08	60 ± 5	1.25 ± 0.10	1.3 ± 0.1
	1.73	*1.73*	*60*	*1.30*	*1.3*
ribbon-type Ib	3.57 ± 0.20	1.92 ± 0.10	80 ± 5	0.84 ± 0.05	2.0 ± 0.1
	3.6	*2.02*	*76*	*0.88*	*1.9*
herringbone Ic	3.30 ± 0.15	4.10 ± 0.15	84 ± 5	0.75 ± 0.05	2.2 ± 0.2
	3.25	*4.04*	*87.5*	*0.73*	*2.3*
linear dimers II	1.43 ± 0.05	1.18 ± 0.05	63 ± 5	0.75 ± 0.02	2.2 ± 0.1
	1.44	*1.15*	*60*	*0.72*	*2.3*
chemisorbed striped phase IIIb	0.86 ± 0.05	2.15 ± 0.20	86 ± 8	0.46 ± 0.05	3.6 ± 0.4
	0.865	*2.00*	*90*	*0.43*	*3.8*

[a] The experimentally determined values are plotted in the first line of each row. The second line (italics) represent the parameter of the theoretical model suggested upon considering the registry between substrate surface and adlayer.

the comparison with the molecular structure of TMA[12] suggest a planar surface orientation. The positions of the symmetrically arranged carboxyl groups in individual TMA molecules are clearly resolved. Adjacent carboxyl groups of each two neighboring TMA units appear to be aligned. Cross-section profiles (Figure 3B) reveal an apparent corrugation height of the bright spots ranging between 0.10 and 0.15 nm and a value of 0.05 nm for the 1.2 nm dark diameter but a somewhat streaky hole in the center. The former represent typical values for physisorbed, planar-oriented aromatic molecules with the π system of the phenyl ring oriented parallel to the substrate surface.[41−45] The planar orientation of TMA in potential region I is also supported by the results of our recent ATR−SEIRAS study.[32]

The highly symmetrical motif shows a characteristic repeat distance of (1.70 ± 0.08) nm. The experimentally determined rhombohedral unit cell with $a = b = (1.70 \pm 0.08)$ nm and $\alpha = (60 \pm 5)°$ is composed of two TMA molecules and gives rise to a coverage $\Gamma_{Ia}(ex) = (1.3 \pm 0.1) \times 10^{-10}$ mol cm^{-2} (Figure 3A, C). These data correspond to $A_{Ia}(ex) = (1.25 \pm 0.10)$ nm^2 as approximate area per molecule (Table 1). The registry between adlayer and substrate could not be determined unambiguously in our experiments. However, the characteristic lengths of the unit cell vectors are close to six times the gold diameter ($6 \times |a_{Au}| = 1.73$ nm). Together with the absence of long-range corrugations (indicative of a Moiré or dislocation pattern) in the TMA phase Ia, we deduce that the molecular layer is commensurate with the substrate and that individual molecules reside at distinct adsorption sites. On the basis of literature data[43,45,46] and a recent ab initio calculation employing density functional theory,[47] we propose that the aromatic phenyl rings of the TMA molecules are preferentially bound to high-symmetry 3-fold hollow sites of the substrate lattice. This assumption suggests a nearly perfect alignment of the (6 × 6) honeycomb-type TMA adlayer to adjacent [110] symmetry directions of the substrate surface. Using vectors of the primitive gold lattice, a_{Au} and b_{Au} (Figure 3C) with $|a_{Au}| = |b_{Au}| = 0.2885$ nm as a basis, one obtains in matrix notation: $\begin{pmatrix} a \\ b \end{pmatrix} = \begin{pmatrix} 6 & 6 \\ 0 & 6 \end{pmatrix} \begin{pmatrix} a_{Au} \\ b_{Au} \end{pmatrix}$. The parameters of the corresponding unit cell are summarized in Table 1.

The comparison of our experimental observations with crystal structure data[12] indicates that the supramolecular honeycomb motif is determined by the hexagonal arrangement of hydrogen-bonded dimers between adjacent carboxyl groups. Each of the three carboxylic acid groups forms two hydrogen bonds with its neighbors. This results in a total of six OH···O hydrogen bonds per TMA molecule, and leads to a strong in-plane stability of the network. The dimer synthon represents the most prevalent hydrogen-bonded pattern formed by aromatic carboxylic acids in the solid state.[9−12] Experimentally, we estimate 0.26 nm as the average length of the OH···O hydrogen bonds. This value is typical for the hydrogen-bonding pattern of carboxylic acid dimers.[10−12,14,48] In the crystal structure of bulk α-polymorph trimesic acid, 1.4 nm diameter holes of the honeycomb exist resulting in a TMA−TMA distance of 1.97 nm through the mesh center and an OH···O bond length of 0.27 nm.[12] The dimensions of the TMA network in the potential region Ia, e.g., at a negatively charged Au(111) electrode, are slightly smaller. This observation could be attributed to the relaxation of the hydrogen bonds in the presence of the electron gas of the charged metal surface. The notion is supported by comparing related hydrogen-bonded assemblies of TMA on different substrate surfaces. Heckl et al. reported on HOPG under UHV conditions[28] and in heptanoic acid[49] a regular physisorbed network with $a = b = (1.72 \pm 0.10)$ nm and $\alpha = (60 \pm 1)°$ as characteristic dimensions of the unit cell. Dmitriev et al. found on Cu(100) substrates at 205 K in UHV small islands of a distorted honeycomb pattern with TMA−TMA distances through the mesh center of $a = 2.04$ nm and $b = 2.28$ nm.[21] Ishikawa et al.[29] obtained for the assembly of 0.1 mM TMA on Au(111)−($p \times \sqrt{3}$) | 0.1 M $HClO_4$ an expanded honeycomb pattern with a hexagonal unit cell of $a = b = 2.3$ nm and $\alpha = 60°$, which is composed of two molecules. Su et al.[30] reported under similar experimental conditions a hydrogen-bonded network, which could be represented by a rhombohedral unit cell with $a = b = 1.15$ nm and $\alpha = 60°$, just containing one molecule. Comparing the properties of the hexagonal honeycomb phase Ia found in the present study with the various open TMA assemblies on other substrate surfaces in solution and under UHV conditions demonstrates that the driving force for the self-assembly process and the dominating intermolecular interactions are the hydrogen

(41) Lippel, P. H.; Wilson, R. J.; Miller, M. D.; Wöll, Ch.; Chiang, S. *Phys Rev. Lett.* **1989**, *62*, 171.
(42) Chiang, S. *Chem. Rev.* **1997**, *97*, 1083.
(43) Sautet, P. *Chem. Rev.* **1997**, *97*, 1097.
(44) Böhringer, M.; Morgenstern, K.; Schneider, W. D.; Berndt, R.; Mauri, F.; de Vita, A.; Car, R. *Phys. Rev. Lett.* **1999**, *83*, 324.
(45) Yuan, H. J.; Lu, J.; Wan, L. J.; Bai, C. L. *J. Phys. Chem.* **2004**, *108*, 11251.
(46) Barth, J. V.; Weckesser, J.; Trimarchi, G.; Vladimirova, M.; de Vita, A.; Cai, Ch.; Brune, H.; Günter, P.; Kern, K. *J. Am. Chem. Soc.* **2002**, *124*, 7991.
(47) Atoderesi, N.; Blügel, S., personal communication, 2005.
(48) Steiner, Th. *Angew. Chem.* **2002**, *114*, 50.
(49) Griessl, S. J.; Lackinger, M.; Jamitzky, F.; Markert, Th.; Hietschold, M.; Heckl, W. *Langmuir* **2004**, *20*, 9403.

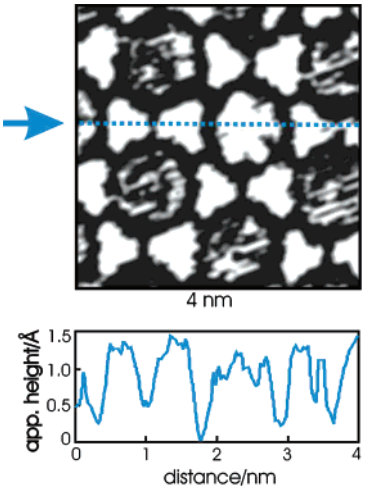

Figure 4. TMA guest molecule positioned in the center of a honeycomb-type hexagonal TMA host lattice, $E_s = -0.10$ V, $i_T = 70$ pA. The line scan represents a typical cross-section profile.

bonds between two carboxylic groups of adjacent TMA molecules. However, interactions of the molecular π orbitals with the substrate surface, with solvent molecules, or with electrolyte ions of the solution phase modify this effect and cause distinct changes.[27−30]

The open 6-fold honeycomb structure with a 1.2 nm diameter "hole" in the center of the ring may act as a nanoscale host system with predefined sites for guest molecules.[15,28,49,50] The formation of size-selective inclusion complexes may significantly increase the packing stability of the hydrogen-bonded pattern. In aqueous electrolyte and in the absence of specific adsorption of anions, the cavities appear streaky (Figures 2A and 3A). These observations are attributed to the high mobility and/or transient adsorption of either water or solute molecules.[51] This interpretation is supported by the absence of similar features in TMA adlayers prepared in UHV.[27,28] Increasing the solution concentration of TMA above 1 mM allows incorporating individual flat-lying physisorbed TMA molecules having a finite residence time in the organic host lattice (Figure 4). The geometry of the latter is not perturbed.

The guest species appear disklike with an apparent corrugation of approximately 0.10−0.15 nm. No triangular features were resolved. The size and shape of the TMA guest molecules indicate no specific interaction, such as directional hydrogen bonds, with the host skeleton. Their smeart-out appearance, in comparison to the regular triangular shape of the two-dimensional host lattice molecules, may indicate a rotation of the TMA guest being significantly faster than the acquisition time of the STM image. A similar interpretation was suggested for coronene incorporated into a TMA host lattice.[49]

3.2.3. Ribbon-Type Motif Ib. Depositing TMA from aqueous electrolyte at higher concentrations ($c > 1.0$ mM) under potential control in 0.00 V < E < 0.20 V reveals large domains of a new two-dimensional assembly pattern of TMA on Au(111)−(1 × 1) and Au(111)−($p \times \sqrt{3}$) (Figure 2, Figure 5). One identifies alternating parallel rows of squares and rhombohedral motifs. Each subunit is composed of four bright spots, which are assigned to individual flat-lying TMA molecules. High-resolution images (Figure 5B) illustrate their regular shape and an apparent corrugation height of 0.10−0.15 nm. The nearest-

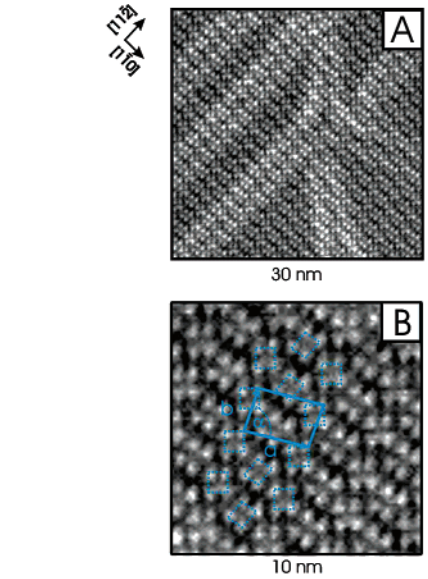

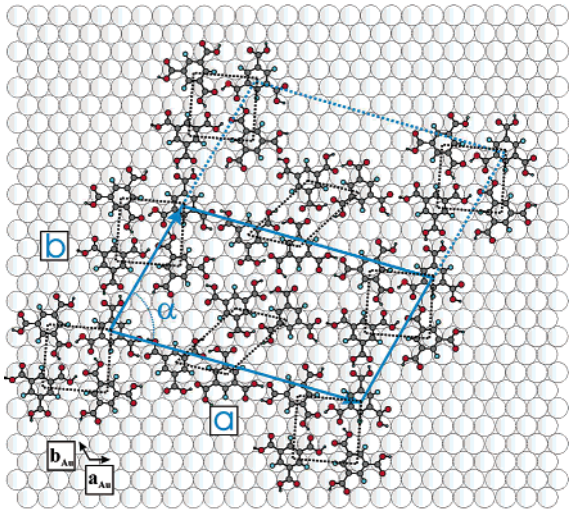

Figure 5. (A) Large-scale in-situ STM image of the ribbon-type motif Ib of TMA on Au(111)−($p \times \sqrt{3}$) | 0.05 M H_2SO_4 in the presence of 3 mM TMA, $E_s = 0.03$ V, $i_T = 150$ pA. (B) High-resolution image of Ib. The unit cell and the characteristic lattice directions on Au(111)−(1 × 1), $E_s = 0.00$ V, $i_T = 160$ pA The characteristic quadratic and rhombohedral structure elements, as well as the primitive unit cell, are indicated. (C) Proposed packing model of TMA in Ib. The parameters of the unit cell are summarized in Table 1.

neighbor distance of the square motif within one row is estimated to $b = (1.92 \pm 0.10)$ nm, and between two adjacent rows of squares to $a = (3.57 \pm 0.20)$ nm. The enclosed angle α amounts to (80 ± 5)°. Within one row, the square units are rotated by (30 ± 3)°, as referenced to the main direction of the row. The same geometrical parameters were obtained from analyzing the rows of rhombohedral-type subunits. The derived unit cell, as drawn in Figure 5B, contains eight individual, flat-lying TMA molecules, which are arranged in alternating rows of quadratic tetramer motifs and parallel dimers in rhombohedral subunits. The area per molecule is estimated to be $A_{Ib}(ex) = (0.84 \pm 0.05)$ nm^2, which corresponds to a coverage $\Gamma_{Ib}(ex) = (2.00 \pm 0.10)\ 10^{-10}$ mol cm^{-2}. Adjacent dimers appear to be aligned with the upper right and the upper left, respectively, the lower right and the lower left TMA molecules in the squared submotif at each corner. The tetramer arrangement is attributed to the formation of a hydrogen-bonded closed loop between the four carboxyl groups of one unit. Similar motifs were

(50) Desiraju, G. R. *Angew. Chem., Int Ed. Engl.* **1995**, *34*, 2311.
(51) Sumetskii, M.; Kornyshev, A. A. *Phys Rev. B* **1993**, *48*, 17493.

reported for the crystal structures of chloroacetic acids[52] and for the self-assembly of 5,10,15,20-tetrakis-(4-carboxylphenyl)-21*H*,23*H*-porphyrin (TCPP) on HOPG.[53] The suggested tetrameric configuration of TCPP was attributed to a compromise between optimal intermolecular hydrogen bonding, maximation of 2D packing, and substrate−adsorbate interaction to minimize surface free energy.[18,53] Crystallographic studies show that the tetramer close-loop motif of carboxylic groups is stabilized by incorporation of water molecules[54,55] or short chain alcohols.[55,56] Returning to the arrangement of dimers in alternating rows of rhombohedral-type subunits, one may assume the typical centrosymmetric motif composed of two carboxyl groups of two neighboring aligned TMA molecules[4,9] or, alternatively, a macrocyclic dimer as formed by four carboxylic groups arranged in 1,3-positions of two adjacent TMA molecules.[22] We hypothesize the preference of macrocyclic dimers on the basis of a molecular modeling approximation with ChemDraw Pro.[57] In this preliminary approach, we considered the planar orientation of TMA in region Ib,[32] the experimentally determined unit cell parameters, space filling arguments, and an attempt to maximize the number of intermolecular hydrogen bonds. Each dimer unit is then allowed to form two respective three hydrogen bonds to adjacent TMA molecules of the tetramer unit. The bond lengths OH···O vary between 0.25 and 0.29 nm with estimated bond angles of 150−180°, typical for strong respective medium-strong hydrogen bonding.[48]

We did not succeed in deriving the registry between the ribbon-type adlayer Ib and the unreconstructed Au(111)−(1 × 1) surface from direct experimental imaging. Fortunately, we found that, within the experimental accuracy, TMA molecules form an identical structure on the reconstructed Au(111)−($p \times \sqrt{3}$) surface in a similar potential range (Figures 1 and 5A). We notice that the adlayer is stabilized inside the reconstruction domains, where the top layer gold atoms occupy fcc and hcp lattice sites (cf. Section 3.3). These experiments also illustrate that the quadratic tetramer motifs are aligned with the [11$\bar{2}$] and the [1$\bar{1}$0] directions of the substrate surface. On the basis of ab initio calculations[47] and experimental results of flat oriented aromatic molecules[27,42,44] we further assume a preferential location of the TMA phenyl ring at or close to energetically favorable 3-fold hollow sites of the hexagonal substrate lattice. Combining both boundary conditions with the above-described tentative properties of a 2D ordered molecular network, we propose the model depicted in Figure 5C for the adlayer Ib. Using vectors of the primitive gold lattice, a_{Au} and b_{Au}, one obtains in matrix notation: $\begin{pmatrix} a \\ b \end{pmatrix} = \begin{pmatrix} 10 & -4 \\ 7 & 7 \end{pmatrix} \begin{pmatrix} a_{Au} \\ b_{Au} \end{pmatrix}$. The model shows typical lengths and angles of intermolecular hydrogen bonding, and nearly all TMA molecules of the unit cell occupy 3-fold substrate coordination sites. The model is in good agreement with the results derived from the experimental images (Table 1, Figure 5C).

Finally we would like to comment on the stability range of the ribbon-type adlayer Ib. Once formed upon assembly from aqueous electrolyte in 0.00 V < E < 0.20 V, the adlayer is stable at negative potentials until $E \geq -0.25$ V, disorders upon partial desorption of molecules, but does not transform into the low-coverage honeycomb network Ia. Increasing the electrode potential causes a structural transition only upon positively charging the electrode surface (cf. Section 3.3).

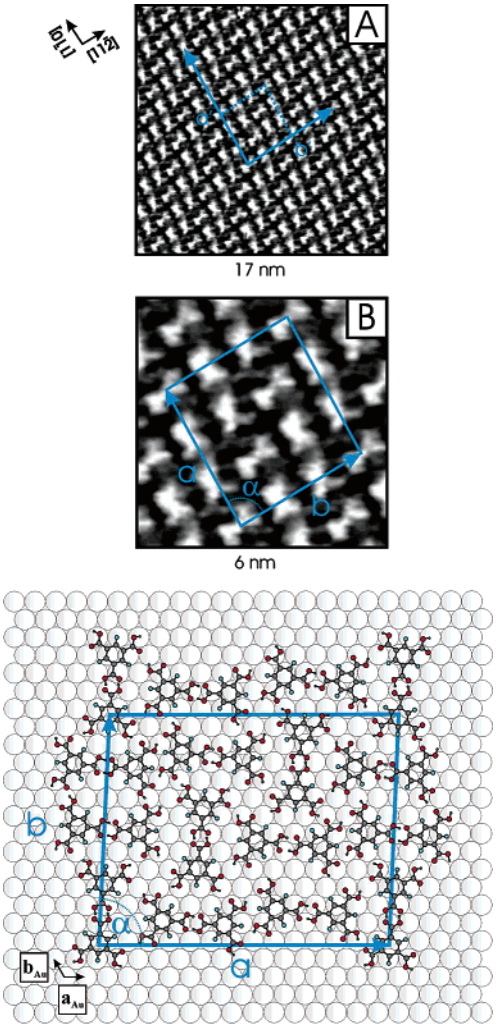

Figure 6. (A) Large-scale in-situ STM image of the herringbone-type motif Ic of TMA on Au(111)−(1 × 1) | 0.05 M H_2SO_4 in the presence of 3 mM TMA, E_s = 0.20 V, i_T = 270 pA. The lattice vectors $\vec{a}'$ and $\vec{b}'$ are indicated. (B) High-resolution image of Ic on Au(111)−(1 × 1), E_s = 0.18 V, i_T = 120 pA. The experimental unit cell is outlined. (C) Proposed packing model of TMA in Ic. The substrate−adsorbate registry is chosen with the assumption to maximize the number of phenyl rings in or close to high-symmetry positions of the substrate lattice. The parameters of the unit cell are summarized in Table 1.

3.2.4. Herringbone Motif Ic. Transient desorption of the ribbon-type motif Ib upon excursion to positive potentials and immediate return to potentials around 0.20 V, e.g., just negative of the capacitive current peaks labeled P1′ respective P1, allows us to create a new two-dimensional long-range assembly of TMA (Figure 2, Figure 6). However, the domains can be easily perturbed by lowering the tunneling resistance (R < 100 MΩ), indicating a rather fragile adlayer phase. High-resolution images reveal a regular arrangement of dimers composed of two triangular units with typical properties of planar-oriented TMA molecules (side length ≈ 0.7−0.8 nm, apparent corrugation height of (0.10 ± 0.02 nm). The length of one dimer-type unit in the STM contrast pattern along the main axis is estimated to (1.4 ± 0.2) nm. These observations and the comparison with the honeycomb motif Ia described be-

(52) Kanter, J. A.; Roelofsen, G. *Acta Crystallogr.* **1976**, *B32*, 3328.
(53) Lei, S. L.; Wang, C.; Yin, S. X.; Wang, H. N.; Xi, F.; Liu, H. W.; Wan, L. J.; Bai, C. L. *J. Phys. Chem B* **2001**, *105*, 10838.
(54) Herbstein, F. H.; Marsh, R. E. *Acta Crystallogr.* **1977**, *B33*, 2358.
(55) Chatterjee, S.; Pedireddi, V. R.; Ranganathan, A.; Rao, C. N. R. *J. Mol. Struct.* **2000**, *520*, 107.
(56) Dale, S. H.; Elsegood, M. R. J.; Richards, S. J. *Chem. Commun.* **2004**, 1278.
(57) *ChemDraw Pro*; Cambridgesoft Corporation: Cambridge, MA, 2000.

fore indicate that the dimers are stabilized by centrosymmetric hydrogen bonds between two carboxyl groups of adjacent TMA molecules.[4,9] Next, we define two adlayer directions by introducing the vectors $\vec{a}'$ and $\vec{b}'$ (Figure 6A). Individual dimers are arranged with their main axis either parallel (represented by "—") or perpendicular (represented by "|") to the introduced adlayer directions. Parallel to the lattice vector $\vec{a}'$, the one-dimensional assembly of TMA dimer units follows the motif "...— | | — | | —...". Parallel to $\vec{b}'$, we identify the motif "...— | — — | — — | —...". The careful inspection of high-resolution STM images demonstrates that the assembly of the four dimers "— | | —" along $\vec{a}'$ and of "| — — |" along $\vec{b}'$ identify the unit cell of the herringbone-type TMA adlayer Ic. The characteristic dimensions along $\vec{a}'$ and $\vec{b}'$ are estimated as $a = (3.30 \pm 0.15)$ nm, $b = (4.10 \pm 0.15)$ nm separated by an angle $\alpha = (84 \pm 5)°$. The complex unit cell is formed by 18 TMA molecules arranged in a regular 2D pattern of centrosymmetric dimers. The area per molecule amounts to $A_{Ic}(ex) = (0.75 \pm 0.05)$ nm^2, and the resulting coverage is given by $\Gamma_{Ic}(ex) = (2.2 \pm 0.2)\ 10^{-10}$ mol cm^{-2}. This value is almost 70% higher than the coverage of the honeycomb network Ia and only slightly higher than the value of the ribbon-type assembly Ib.

The distances and angles between dimers of the same row, as well as of adjacent rows, are compatible with the existence of a complex 2D hydrogen-bonded network. The dimer motif may be considered as a structural element in trimer respective tetramer macrocycles representing motifs of up to four possible intermolecular hydrogen bonds between carboxyl groups of neighboring TMA molecules.[4,9,18,28,50,52,53] A tentative model of the adlayer Ic assumes that the phenyl rings of the TMA molecules are preferentially located in or nearby high-symmetry sites of the hexagonal Au(111)−(1 × 1) substrate. Experimentally we could not determine the exact positions of the aromatic rings with respect to the substrate geometry. Taking the latter assumption, the properties of the experimentally derived unit cell and the geometrical restrictions for dimer, trimer respective tetramer hydrogen-bonding assemblies,[18,53] we propose the model drawn in Figure 6C for the herringbone-type TMA phase Ic. With the primitive vectors of the gold lattice, a_{Au} and b_{Au}, one obtains in matrix notation: $\begin{pmatrix} a \\ b \end{pmatrix} = \begin{pmatrix} 14 & 0 \\ 7 & 13 \end{pmatrix} \begin{pmatrix} a_{Au} \\ b_{Au} \end{pmatrix}$. The tentative assignment is supported by estimations based on molecular modeling with ChemDraw Pro. The model implies a compromise between intermolecular interactions due to hydrogen bonding and adsorbate−substrate interactions to minimize the surface free energy. It is in agreement with the properties of the experimentally observed unit cell (Table 1 summarizes the comparison of the parameters) and maximizes the number of flat oriented TMA molecules localized in "close-to" high coordination 3-fold hollow sites of the Au(111) surface. The model proposes that the $\vec{a}'$ direction of the unit cell is aligned with the $[1\bar{1}0]$ substrate direction. The $\vec{b}'$ vector is misaligned by 2.5° with respect to the $[11\bar{2}]$ direction of Au(111). The experimentally observed "— | | —" and "| — — |" motifs are clearly recognized as subunits of the model structure. The lengths of the hydrogen bonds, OH···O, in the dimer units are typically (0.26 ± 0.01) nm with bond angles of $(180 \pm 5)°$. The lengths of the hydrogen bonds in the trimer and tetramer units appear elongated up to 0.30 nm with estimated angles varying between 150° and 180°.

The herringbone structure Ic dissolves at positive potentials when passing the current peak P1′ in the cyclic voltammograms (Figure 2). On the other hand, it is stable at negative potentials until $E \leq -0.20$ V.

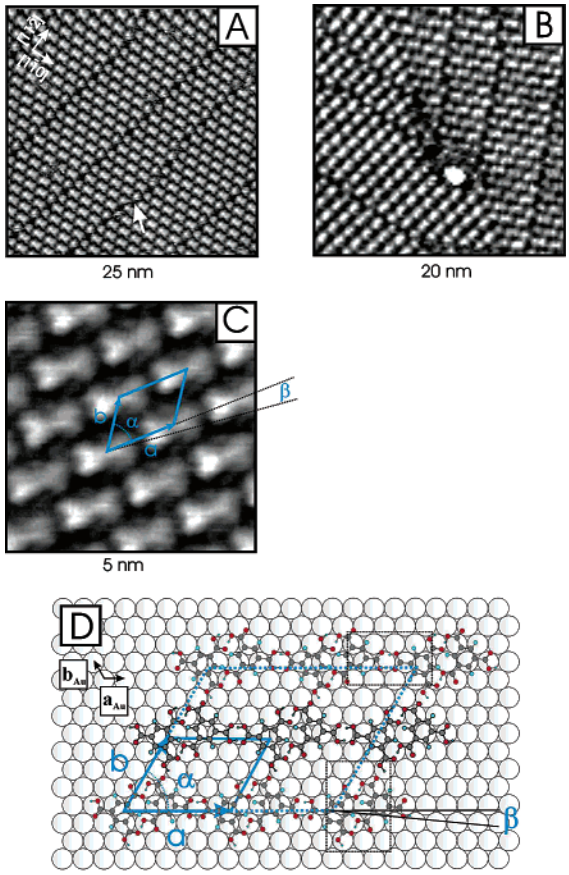

Figure 7. (A) Translational and (B) rotational domain boundaries in a large-scale in-situ STM image of the hydrogen-bonded dimer motif II of TMA on Au(111)−(1 × 1) | 0.05 M H_2SO_4 in the presence of 3 mM TMA, $E_s = 0.33$ V, $i_T = 111$ pA. The arrow in (A) marks a characteristic kink site at a translational domain boundary. (C) High-resolution image of II on Au(111)−(1 × 1), $E_s = 0.30$ V, $i_T = 200$ pA. The primitive unit cell is indicated. (D) Proposed packing model of TMA in II. The parameters of the unit cell are summarized in Table 1.

3.2.5. Hydrogen-Bonded Dimer Motif II. The potential-controlled deposition of TMA ($c > 1$ mM) in $0.20\ \text{V} \leq E \leq 0.40$ V, e.g., in the range marked by the current peaks P1 | P1′and P2 | P2′ in the cyclic voltammograms (Figure 1) triggers the assembly of TMA dimers in quasi-linear rows. The field in the electrical double layer is expected to be small because the electrode bears a rather low excess charge in this potential region.[40] The new adlayer emerges from an initially disordered phase, which slowly transforms, according to a nucleation and growth mechanism, into large two-dimensional islands of the assembly motif II. Characteristic translational and rotational domain boundaries were found (Figure 7A, B). The rotation angles between adjacent domains were $(120 \pm 5)°$ or $(240 \pm 5)°$, thus reflecting the hexagonal symmetry of the substrate surface. Within one adlayer island, one often observes several typically straight and parallel translation domain boundaries. Occasionally, we found kink sites causing steps and a rotation of the domain boundary by 45° (Figure 7A). Identical adlayer structures were detected on Au(111)−(1 × 1) and Au(111)−($p \times \sqrt{3}$). The latter studies indicate that translational domain boundaries often extend over several tens of nanometers and are closely aligned to the $[11\bar{2}]$ direction of the substrate. The width of the corresponding domains in $[1\bar{1}0]$ direction is determined by 2 up to 10 characteristically shaped protrusions

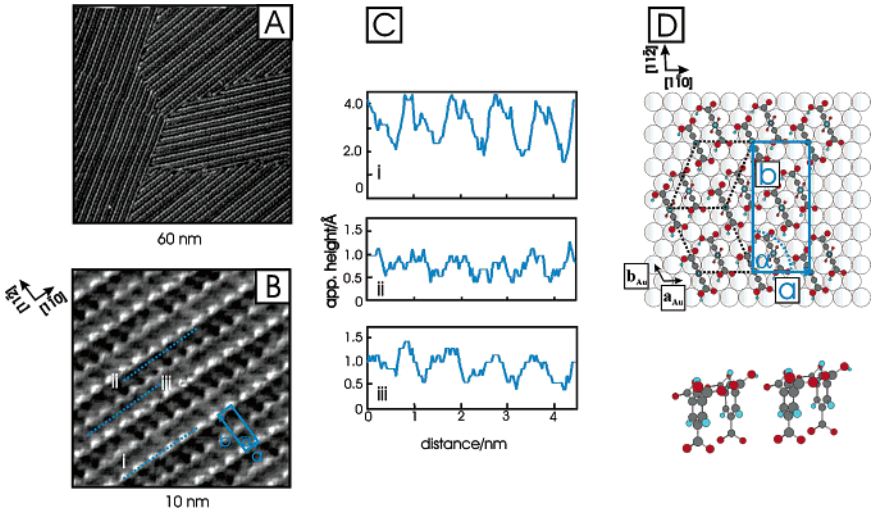

Figure 8. (A) Large-scale in-situ STM image of the chemisorbed striped TMA adlayer IIIb on Au(111)−(1 × 1) | 0.05 M H_2SO_4 in the presence of 3 mM TMA, $E_s = 0.70$, $i_T = 60$ pA. (B) High-resolution image of IIIb on Au(111)−(1 × 1), $E_s = 0.70$ V, $i_T = 77$ pA. The primitive unit cell is indicated. (C) Typical cross-section profile along the directions indicated in (B). (D) Proposed packing model of TMA in IIIb. The parameters of the unit cell are summarized in Table 1.

aligned in parallel and highly correlated one-dimensional chains. Closer inspection (Figure 7C) reveals that they are composed of two triangular features with the typical properties of a planar-oriented TMA molecule (side length 0.7−0.8 nm, apparent corrugation height ≈ 0.08 ± 0.01 nm). Assigning the corners of the triangular spots to the positions of the three carboxyl groups in individual TMA molecules, we conclude on the existence of hydrogen-bonded centrosymmetric dimers.[4,9] TMA dimers within one chain and of entire two-dimensional domains point in the same direction. The centers of these dimers are aligned with the [1$\bar{1}$0] lattice direction. The center-to-center separation is estimated to be $a = 1.43 \pm 0.05$ nm ≈ 5 × $|a_{Au}|$. Moreover, the molecular axis of individual TMA dimers is rotated by $\beta = (5 \pm 2)°$ with respect to the chain direction (Figure 7C). Linear chains of dimers are separated by an inter-row distance of (1.05 ± 0.04) nm. The nearest-neighbor distance between the dimer centers of adjacent rows is estimated to be 1.18 ± 0.05 nm ≈ 4 × $|a_{Au}|$. The regular arrangement of these dimers defines a characteristic second adlayer direction, rotated (63 ± 5)° with respect to [1$\bar{1}$0]. The derived unit cell, which contains two TMA molecules, is indicated in Figure 7C (Table 1). The corresponding area per molecule and coverage were estimated to be $A_{II}(ex) = (0.75 \pm 0.02)$ nm^2 and $\Gamma_{II}(ex) = (2.2 \pm 0.1)\ 10^{-10}$ mol cm^{-2}, respectively. The experimental observations can be rationalized by the directional nature of hydrogen bonding. Molecular modeling (ChemDraw Pro) reveals that the regular arrangement of dimers within one linear row may involve hydrogen-bonded macrocyclic dimers formed between four carboxyl groups of two adjacent TMA units. This motif is known to support the assembly of TMA in planar sheets in three-dimensional supramolecular assemblies.[22] Adjacent TMA molecules of the one-dimensional chains appear to be connected by hydrogen bonds in an alternating arrangement of centrosymmetric and macrocyclic dimers. Single hydrogen bonds may exist between molecules of parallel rows. This hypothesis is supported by the observation that the positions of dimers within one domain appear to be very stable, not frizzy, and highly correlated.[51] Neighboring molecular rows at translational domain boundaries are not in registry. They are in interstitial positions and contain, in an alternating arrangement, TMA monomers with a broken centrosymmetric hydrogen bond. The experimentally observed registry between the linear dimer motif II and the substrate surface suggests a commensurate (5 × 4) TMA adlayer structure. The commensurability of the molecular adlayer II with respect to the substrate is further supported by the absence of long-range corrugations indicative of a Moiré or dislocation pattern. Using vectors of the primitive gold lattice one obtains in matrix notation: $\begin{pmatrix} a \\ b \end{pmatrix} = \begin{pmatrix} 0 & 5 \\ 4 & 4 \end{pmatrix} \begin{pmatrix} a_{Au} \\ b_{Au} \end{pmatrix}$. We further assume that the phenyl rings of the TMA molecules are located in 3-fold hollow sites of Au(111). The corresponding model, depicted in Figure 7D, is in agreement with all experimental observations and gives reasonable values for the OH···O lengths and bond angles of the suggested hydrogen bonded assembly (Table 1). We notice that the substrate−adsorbate interaction (π−ring in 3-fold hollow sites) reduces the distance between the TMA centers of one centrosymmetric dimer by approximately 10%. The model predicts further the misalignment of the dimer axis by −5° with respect to the [1$\bar{1}$0] substrate direction, which results from the directional nature of hydrogen bonds in the alternating arrangement centrosymmetric and macrocyclic dimers.

3.2.6. Chemisorbed Striped TMA Adlayer IIIb. Increasing the electrode potential to higher values, e.g., past the current peak P2 in Figure 2, causes the transformation of phase II previously assigned to hydrogen-bonded linear dimers of TMA (cf. Section 3.3). No ordered structure was found in the potential region between P2 | P2′and P3 | P3′ (region IIIa). For E > P3, where the electrode surface bears a positive excess charge,[40] a long-range ordered and rather fragile new phase labeled IIIb starts to emerge (Figure 8). Individual domains of 50−100 nm size exhibit a characteristic arrangement of alternating bright and dark stripes. Often one observes neighboring domains mutually rotated by integer multiples of 30° indicating a commensurate registry of the adlayer with the hexagonal substrate surface. The striped domains appear to be aligned with one of the [110] substrate directions on Au(111)−(1 × 1). However, when starting the experiment with a reconstructed Au(111)−($p \times \sqrt{3}$) surface, alignment with the [11$\bar{2}$] direction was also found occasionally. High-resolution images such as that shown in Figure 8B reveal details of the striped phase. Rows of identically aligned bright dots (trace (i)) are separated by alternating rows of parallel-aligned light gray (trace (iii)) respective dark gray (trace (ii)) ellipsoidal-like features of 0.7−0.9 nm

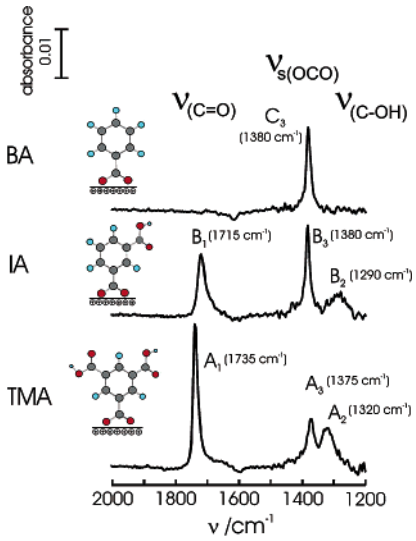

Figure 9. Equilibrium SEIRA spectra of TMA (3 mM), isophthalic acid (IA, saturated solution), and benzoic acid (BA, 3 mM) in 0.05 M H_2SO_4 obtained at 0.80 V in region IIIb. The reference spectra were taken at $E = -0.20$ V. The insets illustrate the derived interfacial orientations of the three molecules chemisorbed on a positively charged Au(111−25 nm) film electrode.

length. Their axis is tilted by 60−70° with respect to the main row directions. Cross-section profiles (Figure 8C) along the row of bright dots (trace (i) in Figure 8B and C) reveal asymmetric main maxima and smaller side maxima with characteristic repeat distances of (0.86 ± 0.05) nm, e.g., neighboring features are approximately three lattice constants apart. The apparent corrugation height is estimated as 0.20−0.40 nm. Adjacent rows of bright dots appear to be slightly darker, while every other row is identical and exactly aligned. The interspacing rows of light and dark features exhibit rather broad maxima of similar periodicity with an apparent corrugation height of 0.05−0.15 nm (Figure 8C, traces (ii) and (iii)). A rectangular repeat motif with $a = (0.86 \pm 0.05)$ nm ($\approx 3|a_{Au}|$) parallel and $b = (2.15 \pm 0.20)$ nm ($\approx 4\sqrt{3}|a_{Au}|$) perpendicular to the bright rows could be identified (Figure 8B, Table 1). The different STM contrast pattern and the increase of the apparent corrugation height in region IIIb indicate an orientation change from flat-lying to a tilted and/or upright-standing configuration accompanied with major changes in the substrate−adsorbate interaction potential. Tunneling may involve molecular σ and π states.[58]

The surface orientation was explored in a comprehensive steady-state and time-resolved study employing surface enhanced infrared reflection absorption spectroscopy (ATR−SEIRAS).[32,40] The detailed study is presented in ref 32. Here we only focus on selected main results (Figure 9). No TMA-related spectral features were found at $E <$ 0.40 V, supporting the notion of flat orientated molecules. In the potential regions IIIa and IIIb, e.g., for $E >$ 0.40 V, three distinct positive-going IR bands appear in the presence of 3 mM TMA at 1720−1735 cm^{-1}, around 1375 cm^{-1}, and at 1300−1320 cm^{-1}.[32] Comparison with solid-state and solution spectra[59,60] supported the assignment of these spectral features to the following TMA vibrations: the stretching mode of C═O in COOH ($\upsilon_{(C=O)}$), the symmetric stretching mode of O−C−O in COO^- ($\upsilon_{s(OCO)}$), e.g., a deprotonated carboxylate group, and the stretching mode of C−OH in COOH ($\upsilon_{(C-OH)}$), respectively. A correlation analysis demonstrates that both sets of vibrations originate from the same molecule. Simultaneously, co-adsorbed, isolated, and strongly hydrogen bonded water was detected. The intensities of the TMA bands increase with positive potential, reach their maximum in the chemisorbed region III, and decrease to zero during the subsequent negative-going scan.[32] Referring to the surface-selection rule of SEIRAS that only vibrations with dipole changes perpendicular to the local surface can be observed,[61] we conclude that perpendicularly oriented TMA molecules could be chemisorbed onto the positively charged electrode surface via one or two deprotonated carboxylate groups. An orientation change from flat-lying to an upright-standing conformation takes place following deprotonation of the TMA carboxyl group(s) due to the strong interaction of the negatively charged carboxylate ion with the positively charged electrode.[32] TMA forms a distinct chemisorption bond. The corresponding gain in chemisorption energy with the upright geometry is assumed to compensate for the loss of the π bonding upon reorientation of the flat-lying species. Carboxylate formation is a typical finding on a positively charged electrode surface in contact with aqueous electrolyte.[62−64] To resolve the issue on surface coordination, we carried out a comparative study of TMA with benzoic acid (BA) and isophthalic acid (IA) in the high-coverage region.[32] These carboxylic acids have different numbers of identical carboxyl groups but similar conjugated structures. Figure 9 shows typical SEIRAS equilibrium spectra of the three molecules at $E = 0.80$ V. The comparative correlation and intensity analysis of the observed carboxylate modes and of the vibrations attributed to protonated carboxyl groups provide clear evidence for deprotonation and surface coordination of only one carboxylate group of TMA. The remaining two protonated carboxyl side groups are directed toward the electrolyte and may form intermolecular hydrogen bonds.[32] On the basis of calculations and experimental evidence for related systems,[27,58,62−68] we suggest that the surface-bound carboxylate group is centered at 2-fold short bridge sites. The carbon atom resides midway between two nearest-neighbor gold atoms, and the chemically bound oxygen atoms are equivalent from the surface. TMA forms a distinct chemisorption bond. The site-specificity, a consequence of a strong, localized surface−molecule bond and interaction through a single molecule functionality contrasts with the behavior of the flat-lying species with their multifunctional surface interaction.[66] The phenyl ring and the protonated carboxyl groups may undergo conformational rotations with respect to C−C bonds which allows forming a supramolecular network stabilized by intermolecular hydrogen bonding involving the solution-directed carboxyl groups. The analysis of potential-induced time-dependent SEIRAS experiments demonstrated[32] that the formation of chemi-

(58) Frederick, B. G.; Chen, Q.; Leibsle, F. M.; Lee, M. B.; Kitching, K. J.; Richards, N. V. *Surf. Sci.* **1997**, *394*, 1.
(59) Arenas, J. F.; Marcos, J. I. *Spectrochim. Acta* **1979**, *35A*, 355.
(60) Gonzalez; Sanchez, F. *Spectrochim Acta* **1957**, *12*, 17.
(61) Osawa, M. *Bull. Chem. Soc. Jpn.* **1997**, *70*, 2861.
(62) Ikezawa, Y.; Sekiguchi, R.; Kitazume, T. *Electrochim. Acta* **2000**, *46*, 731.
(63) Noda, H.; Wan, L. J.; Osawa, M. *Phys. Chem. Chem Phys.* **2001**, *3*, 3336.
(64) Noda, H.; Ataka, K.; Wan, L. J.; Osawa, M. *Surf. Sci.* **1999**, *427−428*, 190.
(65) Frederick, B. G.; Ashton, M. R.; Richardson, N. V.; Jones, T. S. *Surf. Sci.* **1993**, *292*, 33.
(66) Frederick, B. G.; Leibsle, F. M.; Haq, S.; Richardson, N. V. *Surf. Rev. Lett.* **1996**, *3*, 1523.
(67) Casarin, M.; Granozzi, G.; Sambi, M.; Tondello, E. *Surf. Sci.* **1994**, *307−309*, 95.
(68) Ortega-Lorenzo, M.; Baddeley, C. J.; Muryn, C.; Raval, R. *Nature* **2000**, *404*, 376.

sorbed TMA in phase IIIb proceeds in two steps: TMA molecules change their orientation from planar to perpendicular accompanied by the deprotonation of one carboxyl group after a potential step toward positive charge densities. In a subsequent and much slower process, the chemisorbed TMA molecules start to gradually align into a highly ordered two-dimensional network IIIb (cf. Section 3.3).

On the basis of complementary observations from in-situ STM and ATR−SEIRAS experiments, we propose the model depicted in Figure 8D for the adlayer of chemisorbed TMA on Au(111)−(1 × 1) in the potential region IIIb. The structure is represented by a commensurate (3 × 4√3) unit cell. Using vectors of the primitive gold lattice, a_{Au} and b_{Au}, as the basis, one obtains in matrix notation: $\begin{pmatrix} a \\ b \end{pmatrix} = \begin{pmatrix} 3 & 0 \\ 4 & 8 \end{pmatrix} \begin{pmatrix} a_{Au} \\ b_{Au} \end{pmatrix}$. The unit cell is composed of four molecules. The corresponding area per molecule and coverage obtained were $A_{IIIb}(th) = 0.43$ nm^2 and $\Gamma_{IIIb}(th) = 3.8\ 10^{-10}$ mol cm^{-2}, respectively. The bright dots along [1$\bar{1}$0] are assigned to pairs of upright and parallel-aligned TMA molecules coordinated to the positively charged substrate surface via one deprotonated carboxylate group per molecule. The aromatic ring and the carboxylate group of one molecule assume a coplanar conformation. A 30° rotation of the carboxylate plane is suggested for the second TMA molecule of the pair. The surface-bound carboxylate groups of both molecular units are in registry with the direction of the hexagonal substrate in energetically favored bridge sites. The parallel orientation of the phenyl ring and their alignment with the rows of densely packed gold atoms within one pair is supported by the possible formation of intermolecular hydrogen bonds involving the solution-directed protonated carboxyl groups. In this arrangement, the parallel phenyl rings of one dimer are separated by 0.375 nm (=$^3/_4\sqrt{3}|a_{Au}|$) and the distance between the displaced centers of carboxylate groups amounts to 0.38 nm (=$^1/_2\sqrt{7}|a_{Au}|$). Nearest-neighbor parallel rows of bright dots, which appear slightly darker in the experimental STM image, are also assigned to pairs of upright TMA molecules, exhibiting just the reverse alignment of phenyl ring and coordinating carboxylate. The two types of alternating molecular rows are separated by 1 nm (=$2\sqrt{3}|a_{Au}|$) in the [11$\bar{2}$] direction. The bright features in neighboring rows representing pairs of molecules are mutually shifted by 0.43 nm (=$3/2|a_{Au}|$) along the [1$\bar{1}$0] direction. This arrangement enables still the existence of inter-row hydrogen bonding. Each TMA molecule may form up to four hydrogen bonds with molecules ("or molecular dimers") within the same and of neighboring rows, thus giving rise to a supramolecular ladder-type network. On the basis of X-ray crystal structure data[12] and molecular modeling with ChemDraw Pro, hydrogen-bond lengths ranging between 0.26 and 0.30 nm are estimated. The interspacing rows of light gray and dark gray ellipsoidal features between the rows of bright dots, as illustrated in the STM contrast pattern in Figure 8B, might result from aligned carboxyl groups and/or mutually shifted phenyl rings of pairs of dimers. On the basis of our experimental data only, we can not suggest a more specific assignment. We aim to investigate the geometrical and electronic structure of the carboxylate-anchored molecular adlayer in more detail applying density functional (DFT) calculations based on a projector augmented plane-wave package.[47]

3.3. Structural Transitions−Dynamic Processes. The steady-state experiments demonstrated that, depending on the applied electrode potential, up to five ordered TMA adlayers could be assembled on Au(111)−(1 × 1)/0.05 M H_2SO_4. The coverage increases upon polarizing the electrode surface from negative to positive charge densities accompanied by an orientation change from planar (Ia, Ib, Ic, II) to upright (IIIb). We also notice that the three structures Ia (honeycomb), Ib (ribbon-type), and Ic (herringbone-type), once formed upon potential-controlled assembly at the Au(111) | electrolyte interface, do not transform mutually into each other by tuning the electrode potential within an observation time of up to 4 h. However, structural transitions could be triggered if the final potential was chosen in the potential regions II or III, respectively.

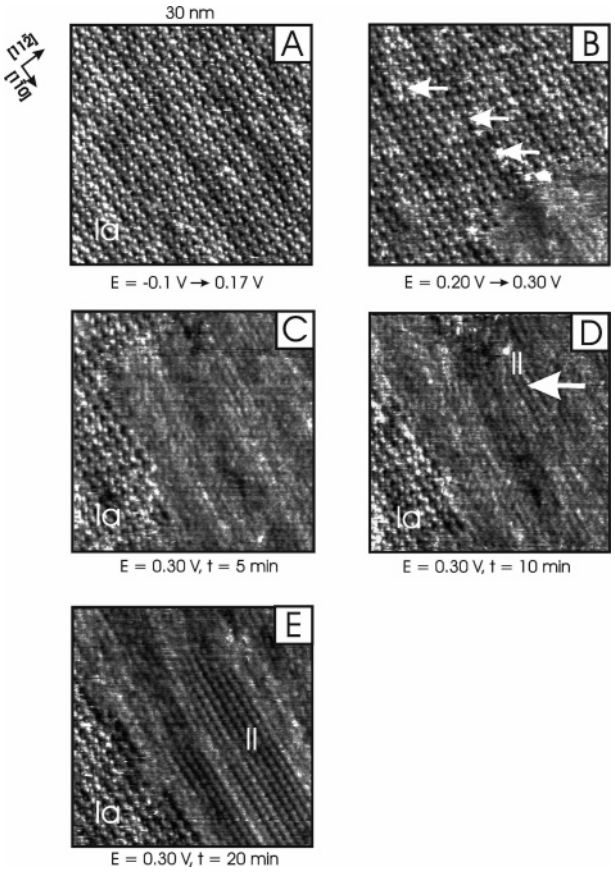

Figure 10. STM images (30 nm × 30 nm) for Au(111) | 0.05 M H_2SO_4 in the presence of 3 mM TMA after a sequence of potential steps from $E_s = -0.10$ V (stability range of the hexagonal honeycomb phase Ia) to $E_s = 0.30$ V (stability range of the hydrogen-bonded dimer phase II), $i_T = 120$ pA. The formation of active "hole" nucleation sites is indicated by white arrows.

Figure 10 illustrates the dissolution of the long-range ordered honeycomb phase Ia and the subsequent evolution of the linear dimer motif II after a series of potential steps from $E_i = -0.10$ V to $E_f = 0.30$ V (Figure 10). The process starts with the appearance of "frizzy spots" indicating a local enhancement in the mobility of the hydrogen-bonded network Ia (cf. arrows in Figure 10B). The active sites are evenly distributed across entire terraces without specific preferences to defects of the adlayer or substrate lattice. Subsequently, they transform into islands of a disordered pattern, such as that indicated in the right lower corner of Figure 10B. Growth proceeds preferentially along the symmetry directions of the molecular adlayer Ia, which are in registry with the substrate surface. The transient phase appears fluidlike with a distinct local order (Figure 10C, D). However, no patterns resembling the motifs Ib or Ic could be identified. After an induction period, parallel lines of linear dimers, the adlayer motif II, start to grow

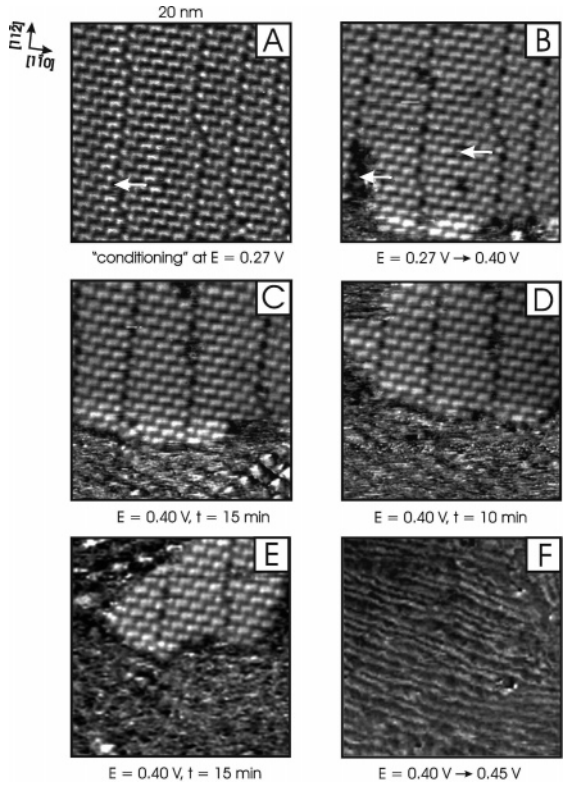

Figure 11. Sequence of STM images (20 nm × 20 nm) for Au(111) | 0.05 M H_2SO_4 in the presence of 3 mM TMA after a potential step from E_s = 0.27 V (stability range of the linear dimer phase II) to E_s = 0.45 V (stability range of the disordered chemisorbed stripe phase IIIa), i_T = 82 pA. White arrows indicate the formation of active sites of the structural transformation.

along the [1$\bar{1}$0] symmetry direction of the substrate surface (first islands in Figure 10D and larger areas in Figure 10E). Adjacent patches of Ia and II are separated by disordered regions. No complete transformation could be achieved, most probably related to kinetic limitations due to uncorrelated domains of the two ordered phases and/or to the slow movement of domain walls.[69] The transformation into the disordered chemisorbed adlayer IIIa starts at higher positive potentials (Figure 11), while the excursion to negative potentials leads to the reformation of the honeycomb phase Ia.

Once the hydrogen-bonded dimer motif II is formed by potential-controlled self-assembly from electrolyte solution on Au(111)−(1 × 1) (stability range delimited by the pairs of current peaks P1 | P1′ and P2 | P2′), it can be transformed at E < P1′ into the herringbone phase Ic and at E > P2 into the disordered, chemisorbed adlayer IIIa (Figure 11). The later process starts at adlayer defects on terraces but most frequently on translational domain boundaries. These local sites are composed of planar-oriented TMA monomers (Figure 11A, B). The latter are less strongly stabilized by the two-dimensional hydrogen-bonded network in region II. Subsequently, the linear dimers dissolve anisotropically line-by-line. The dissolution rate parallel to the chains of linear dimers, which are aligned to the [1$\bar{1}$0] substrate direction, is faster than the process perpendicular to these rows. The newly formed adlayer IIIa is composed of rather fragile and irregular one-dimensional features, which start aligning at higher positive fields into a disordered chemisorbed striped phase.

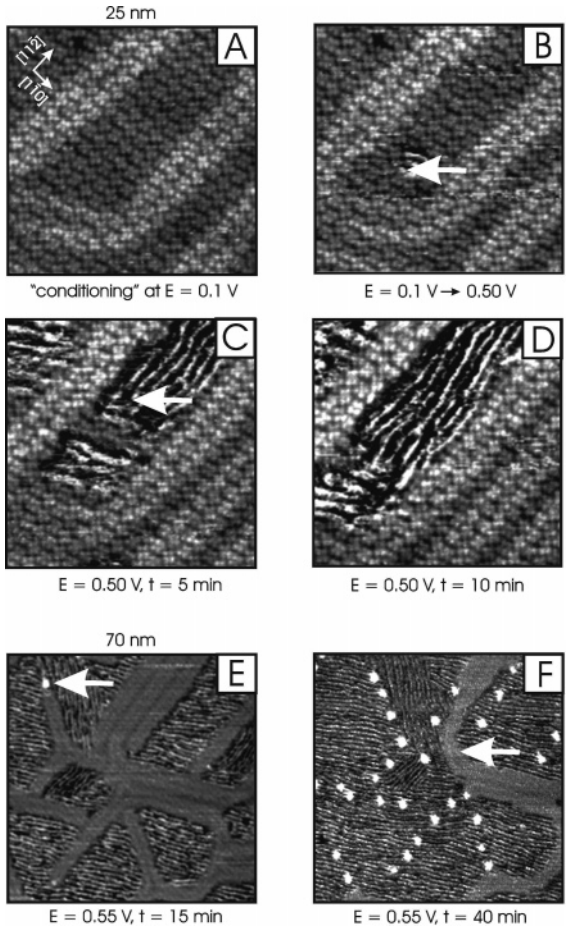

Figure 12. Sequence of STM images (25 nm × 25 nm, 70 nm × 70 nm) for Au(111)−($p \times \sqrt{3}$) | 0.05 M H_2SO_4 in the presence of 3 mM TMA after a potential step from E_s = 0.10 V (stability range of the ribbon-type motif Ib) to E_s = 0.50 V (A, B, C, D) respective E_s = 0.55 V (E and F, stability range of the disordered chemisorbed stripe phase IIIa), i_T = 82 pA. White arrows indicate the formation of active sites (B, C) of the structural transformation, as well as of monatomic gold islands due to he lifting of the substrate surface reconstruction (E, F). i_T = 170 pA.

Complementary IR spectroscopic investigations revealed that this transition involves an orientation change of TMA molecules from planar to perpendicular, accompanied by the deprotonation of *one* COOH− group that is chemically bound to the positively charged electrode. The formation of a highly ordered two-dimensional network of chemisorbed TMA molecules, IIIb, as found for the direct assembly from electrolyte solution (Figure 8), appears to be hindered kinetically. Possible reasons are the high surface coverage in the initial adlayer of planar-oriented molecules (up to Γ_{II}(ex) = 2.2 10^{-10} mol cm^{-2}), as well as the low mobility of chemisorbed TMA. Similar observations were reported previously for uracil and thymine on Au(111).[33,70,71] Stepping the potential toward negative values triggers the reformation of hydrogen-bonded dimers (P1/P1′ < E_f < P2/P2′) or one of the ordered phases described previously in region I (E < P1/P1′).

Finally, we report on the role of the Au(111)−($p \times \sqrt{3}$) surface reconstruction. All hydrogen-bonded adlayers of planar-oriented TMA molecules (Ia, Ib, Ic, and II) were also found on the thermally and electrochemically recon-

(69) Meakin, P.; Cardy, J. L.; Loh, E.; Scalapino, D. J. *J. Chem. Phys.* **1987**, *86*, 2380.

(70) Dretschkow, Th.; Dakkouri, A.; Wandlowski, Th. *Langmuir* **1997**, *13*, 2843.

(71) Li, W. H.; Haiss, W.; Floate, S.; Nichols, R. J. *Langmuir* **1999**, *15*, 4875.

structed Au(111)−($p \times \sqrt{3}$) electrodes. We estimated dimensions of the respective unit cells to be identical to the results obtained with Au(111)−(1 × 1) within experimental error. However, we also discovered that the physisorbed adlayers of planar-oriented hydrogen-bonded TMA molecules are stabilized within the reconstruction domains, where the top-layer gold atoms occupy hcp and fcc lattice sites. An example is given in Figure 12. The ribbon-type adlayer Ib was assembled via direct deposition from aqueous solution at $E = 0.10$ V on an electrochemically reconstructed surface. Alternating rows of squares and rhombohedral motifs are aligned with the [11$\bar{2}$] substrate direction. Stepping the potential to $E_f = 0.50$ V, e.g., to positive charge densities in region IIIa, causes the formation of hole nuclei only on unreconstructed patches of the Au(111) surface (Figure 12B). These activated sites initialize the growth of the disordered chemisorbed striped phase IIIa. Individual stripes of the newly formed adlayer are typically aligned with one of the neighboring reconstruction lines parallel to the [11$\bar{2}$] substrate direction. No disintegration of the hydrogen-bonded physisorbed adlayer was found on the reconstructed patches (Figure 12D, E). Upon further increasing the electrode potential to positive potentials, one triggers the lifting of the surface reconstruction as indicated by the appearance of gold island in Figure 12E. The local reconstruction is lifted with progressing observation time resulting in the formation of many monatomic high gold islands. Their size is rather constant, ∼5 nm, and they seem to decorate exactly the directions of the previously existing reconstruction elements. This observation demonstrates that the gold islands just contain atoms, which are released from adjacent lattice positions of the previously reconstructed substrate, and immediately after this step their further mobility is "frozen". The abrupt blocking is caused by the chemisorbed phase IIIa, which appears only on unreconstructed Au(111)−(1 × 1) sites. The formation of gold islands induces a distinct disorder within phase IIIa, which prevents the growth of the long-range ordered chemisorbed striped phase IIIb, even at significantly higher electrode potentials. Similar observations were also obtained when starting the experiment with the honeycomb or the herringbone phases Ia respective Ib on Au(111)−($p \times \sqrt{3}$).

4. Summary and Conclusions

We have studied the potential-controlled self-assembly of TMA, a benzene-derived polycarboxylic acid, on Au(111) in contact with aqueous 0.05 M H_2SO_4 at room temperature. Carboxylic acids in general and TMA in particular are known to form in the crystalline phase diverse patterns of intermolecular hydrogen bonding. Adsorption on a surface may impose additional significant contributions from substrate−adsorbate interactions. The interactions of benzene-derived π-bonded molecules with densely packed surfaces of noble metals such as Au(111) appear to be weak but distinct. The phenyl ring of TMA determines the registry with the substrate surface, while the symmetrically arranged carboxyl side groups induce chemical functionality. The electrochemical environment allows us to steer the molecular self-assembly and to establish equilibrium structures by the subtle variation of the externally applied electric field.

At negative charge densities and in the absence of an applied field, individual molecules appear in the STM contrast pattern as bright equilateral triangles, which reflect a flat-lying geometry with the phenyl ring parallel to the substrate surface. The symmetry and the characteristic side lengths of approximately 0.7−0.8 nm agree well with geometrical shape and dimensions of TMA. The π-conjugated phenyl rings and the positions of the carboxyl groups are expected to exhibit high contrast in the STM images.[42−45] The flat surface orientation is further supported by the apparent corrugation heights ranging between 0.10 and 0.15 nm, which are typical values for physisorbed aromatic molecules with their π system parallel to the substrate surface. On the basis of experimental evidence and theoretical predictions, we propose that the aromatic phenyl rings of TMA are preferentially bound to 3-fold hollow sites of the Au(111) lattice. Four long-range ordered, commensurate adlayers with distinct two-dimensional packing motifs were found, which we labeled honeycomb (Ia), ribbon-type (Ib), herringbone-type (Ic), and linear dimer (II) phases. The commensurability reflects the non-negligible interactions with the Au(111) surface. All adlayers are rather fragile. They can be easily perturbed upon lowering the tunneling resistance below 100 MΩ, despite the existence of long-range ordered domains and low defect density. A basic element or "synthon" of all these structures represents centrosymmetric hydrogen-bonded dimers formed between two carboxyl groups of two aligned TMA molecules. The honeycomb pattern, which only exists at a negatively charged electrode surface, is exclusively composed of hydrogen-bonded dimers between adjacent carboxyl groups. Their hexagonal arrangement is determined by the trigonal geometry of TMA. The packing of the open ring structure appears to be stabilized by the transient adsorption of water and/or additional TMA molecules as guest species into the nanoscale cavities.

The potential-controlled deposition of TMA at less-negative charge densities leads to planar-oriented hydrogen-bonded assemblies composed of ribbon-type (Ib) and herringbone-type (Ic) motifs. The surface coverage increases up to 70%. The proposed structure models suggest a complex but regular arrangemt of centrosymmetric hydrogen-bonded TMA dimers, together with macrocycles composed of two, three, or four individual molecules. These two-dimensional networks appear to be a compromise between an optimum geometry of hydrogen-bonding, increasing substrate−adsorbate interactions, and minimization of surface free energy. The increase of surface packing is energetically favorable.

The hydrogen-bonded trimer and tetramer macrocycles are not stable if the external electric field is rather small. Around the potential of zero charge, TMA molecules form one-dimensional chains composed of an alternating arrangement of centrosymmetric and macrocyclic hydrogen-bonded dimers. Neighboring chains are correlated giving rise to highly ordered two-dimensional sheets. Molecular modeling suggests the existence of interchain hydrogen bonding.

Increasing the electrode potential further to positive charge densities of Au(111) destabilizes all hydrogen-bonded networks of flat adsorbed TMA molecules, and an orientation change from planar to upright takes place. One observes initially a disordered chemisorbed adlayer, IIIa, which transforms at higher potentials into the mesoscopically long-range ordered striped phase, IIIb. The process was monitored by combining in-situ STM and SEIRAS[32] (surface enhanced infrared reflection−absorption spectroscopy): TMA molecules change their orientation from planar to upright accompanied with the deprotonation of one carboxyl group. Subsequently, this carboxylate group coordinates to the positively charged electrode surface while the two other carboxyl groups are directed toward the electrolyte. This arrangement supports the formation of a long-range ordered supra-

molecular ladder-type network, which is structurally determined by substrate−adsorbate coordination and lateral hydrogen-bonding.

The present study demonstrates at a molecular level the tuning possibilities of an externally applied electric field in controlling adsorbate−adsorbate and substrate−adsorbate interactions during the self-assembly of equilibrated supramolecular nanostructures at electrified solid/liquid interfaces. The TMA experiments reveal three aspects of general importance for the assembly of carboxylic acid-based architectures at electrified metal/solution interfaces: (1) Applying a positive filed (positive charge at the substrate!) causes the deprotonation of at least one of the carboxyl groups, which leads to the formation of substrate−adsorbate coordination compounds. The structure and stability of these assemblies depends strongly on the other molecular functionalities and on the co-deposition of solution components (solvent molecules, ions, ...). (2) The positive field also triggers the alignment of the main molecular dipole axis parallel to the field direction and destabilizes hydrogen-bonded networks. (3) Both phenomena were not observed at negative charge densities. Gaining control of two-dimensional pattern formation represents a crucial step in designing functional surfaces. Tailored well-defined nanoscale building blocks at electrified interfaces may provide unique new strategies and insight to fabricate and to address molecular nanostructures. The electrochemical approach is just at its beginning.

Acknowledgment. The work was supported by the Volkswagen Stiftung under Grant No. I77-116 and the Research Center Jülich. The authors also acknowledge the skilful preparation of stepped gold single crystals by U. Linke and the help of H. Bierfeld in preparing the gold film electrodes. L.J.W. acknowledges support from the National Science Foundation of China.

LA0507737